Real Space Ab Initio Molecular Dynamics Simulations for the Reactions of OH Radical/OH Anion with Formaldehyde

Hideaki Takahashi,* Takumi Hori, Tadafumi Wakabayashi, and Tomoshige Nitta

Division of Chemical Engineering, Graduate School of Engineering Science, Osaka University, Toyonaka Osaka 560-8531, Japan

Received: November 30, 2000; In Final Form: February 21, 2001

A real space ab initio molecular dynamics method reinforced by the double grid technique has been applied to the simulations of the reactions of OH radical/OH anion with formaldehyde to examine their reactivities and also to test the efficiency of the method. The simulation revealed that the H-abstraction reaction by the OH radical takes place without potential energy barriers within the level of generalized gradient approximation (GGA). The heat of the reaction computed by a gradient-corrected functional is 33.3 kcal/mol, which is in good agreement with the experimental value of 33.2 kcal/mol. The molecular dynamics of the formation of tetrahedral complex $[HCHO-OH]^-$ in the ionic process has also been found. The optimized structure of the complex was compared with those obtained by MP2 and BLYP calculations by Gaussian 98, which showed excellent agreement.

I. Introduction

The ab initio electronic structure calculation has become a fundamental method in recent years in the studies of chemistry and physics supported by the rapid growth of computational ability. The density functional theory (DFT) approach coupled with the pseudopotential and planewave basis is one of the most successful methods of the ab initio calculations for the periodic systems.[1−4] In recent years, a number of works that employ real space grids have been proposed to expand electronic wave functions.[5−8] The real space grid approach has several advantages compared with the planewave basis approach. First of all, it can treat nonperiodic system such as clusters or charged systems as well as semiperiodic systems straightforwardly. Within the plane wave basis approach, it is not trivial to get rid of the periodicity though a solution was given.[9] Second, it is straightforward to augment dense real space grids *only* near the atomic core region where the nonlocal pseudoptential varies rapidly. Such a spatially localized augmentation of the basis functions is impossible when the planewave basis sets are employed since they are spatially delocalized. The third is that one can drastically reduce the number of fast Fourier transformations (FFT) that are required for each occupied molecular orbital because only total electron density must be transformed by FFT and it becomes more amenable to parallel implementations. FFTs involve nonlocal operations that make it difficult to divide a system into localized domains that are to be distributed over parallel computers. Further, in the real-space grid approach, the localized nature of the Hamiltonian operations enables us to divide the system into domains without the substantial increase in the amount of communications between processors. Several big challenges for large-scale electronic structure calculations were carried out using massively parallel computers within the real-space grid approach.[10−14]

A drawback of the real space grid method is that the relative position of an atom with respect to grid points will seriously affect the results of the computations unless the grid spacing is narrow enough. That is because a pseudopotential varies so rapidly near the atomic center that the grid points could not represent accurately the variation of the pseudopotential. One of the promising ways to conquer this problem is to prepare dense grid points near the atomic core region, which leads to a high degree of accuracy; however, it causes the increase of the computational cost as well as computer storage. Recently, Ono and Hirose proposed a quite simple and efficient double-grid technique that requires only a modest increase of computational cost without a loss of accuracy in the framework of the real space finite-difference method.[15] In the previous report, we have proved that the real space grid augmented by a dense grid near the atomic core regions can yield a rather weak interaction, hydrogen bond energy of the water dimer successfully.[16]

Despite the many advantages of the real space grid method, its applications to the investigations of physical or chemical problems can be scarcely found.[10−14] Most of the applications are treated by the planewave basis approach and the rest of them by the linear combination of the atomic orbitals (LCAO) method.[17−33] In this work, we apply the real space grid method to the simulations of chemical reactions by the ab initio molecular dynamics (AIMD) method pioneered by Car and Parrinello.[29] The AIMD approach enables us to simulate the chemical reactions that involve the bond formations or breakings during the course of the molecular dynamics because the forces acted on the nuclei are explicitly determined from the electronic density of the ground state. In the present application of the real space grid approach, we use the double grid method proposed by Ono and Hirose.

The major purposes of the present real space ab initio molecular dynamics (RS-AIMD) simulation are to examine the reaction of the OH radical and OH anion with an organic molecule to get insight into their reactivity under the supercritical

* Corresponding author. E-mail: takahasi@cheng.es.osaka-u.ac.jp. Fax: 81-6-6850-6265.

10.1021/jp004348s CCC: $20.00
Published on Web 04/07/2001

conditions of water and further to test the applicability of the real space grid method to the AIMD simulations. Supercritical water (SCW) is well-known as a strong reaction field, and there has been much literature that deals with the organic chemical reactions in water near or above its critical point.[34] In ref 34 it is pointed out that the ion product, or the dissociation constant for water, increases as the temperature approaches the critical point but decreases dramatically as the temperature exceeds the critical point. As a reason for the high reactivity of the SCW, the water molecule will possibly behave as a reactant itself rather than a passive solvent. We can speculate that ionic or radical species (OH^-, H^+, $OH^\bullet$, $H^\bullet$) that come from water molecules are so rich in a certain condition of water that the organic reactions are promoted. This speculation gives rise to the question which process, radical or ionic, is more advantageous for reactions in the SCW? In ref 35 it is reported that HCOOH is produced from formaldehyde in hot water without a catalyst. In this paper, we consider following radical and ionic reaction processes of formaldehyde, which both lead to the same product HCOOH.

radical process

$$HCHO + OH^\bullet \rightarrow CHO^\bullet + H_2O$$

$$CHO^\bullet + OH^\bullet \rightarrow HCOOH$$

ionic process

$$HCHO + OH^- \rightarrow [HCHO\cdots OH]^-$$

$$HCHO + [HCHO\cdots OH]^- \rightarrow HCHO^- + HCOOH$$

The first process is composed of the electrophilic attacks of OH radical. The ionic process is known as a kind of Cannizzaro reaction, the first step of which is the nucleophilic addition of the OH ion.

In this work we focus on the first step of each reaction to clarify the difference in the dynamics, energetics, and reactivity between radical and ionic process and to get more insight into the origin of the high reactivity of the SCW. In principle, one should consider possibilities of other reaction pathways, for example, addition of the OH radical or H-abstraction by the OH anion, etc.; however, the above two pathways are undoubtedly the simplest radical and ionic processes that lead to HCOOH formation. Therefore, it will be appropriate to consider these pathways as most probable candidates unless they require unexpectedly large activation energies as compared with given temperature. One can find some experimental and theoretical literature related to these reactions.[36−46] The H-abstraction reaction of the OH radical is known as a combustion reaction and has been investigated by spectroscopic experiment.[36] In ref 45 static molecular orbital calculations of the addition of nucleophiles to formaldehyde have been performed and the heat of reaction is computed by using rather small Gaussian basis sets at MP2 and SDCI levels. Unfortunately, these studies were separately done and no comparison on the energetics was made on the basis of the same level of the quantum chemical calculations. In addition, the authors cannot find any molecular dynamical information on the reaction processes in the literature although the reaction of the carbonyl group plays a vital role in organic and biological chemistry.

In solution, water solvent will play a significant role in determining the reaction paths; however, at high temperatures near or above the critical point the solvation effects of water molecules will be substantially diminished because most of the intermolecular bondings are broken. It is therefore necessary to investigate the reactions under the isolated conditions to understand the intrinsic factors that control the reactivity of the OH radical and ion. On the basis of this consideration, we performed the simulations with no solvent water molecules as the first step of investigations of reactions in the SCW.

II. Method

The electronic ground state of the system is computed by the Kohn−Sham density functional scheme. The Kohn−Sham equation for the orbital φ_i with eigenvalue ϵ_i of the system can be written as

$$\left[-\frac{1}{2}\nabla^2 + \int \frac{\rho(\mathbf{r})}{|\mathbf{r}-\mathbf{r}'|}\,d\mathbf{r}' + \nu_{ps}(\mathbf{r}) + \nu_{xc}(\mathbf{r})\right]\psi_i = \epsilon_i\psi_i \quad (1)$$

where the first term inside the parentheses is the kinetic energy operator, the second is the Hartree potential, the third is the pseudopotentials of the atoms, and the fourth is the exchange and the correlation functional, respectively. In our calculations we use real space grids to expand wave functions and employ the fourth-order finite difference method to represent the kinetic energy operator.[5−8] The Hartree potential is computed in the Fourier space. The nonlocal atomic pseudopotentials are separated into a local potential and the Kleinman−Bylander nonlocal form in a real space,[47]

$$\nu_{ps}(\mathbf{r})|\psi_i\rangle = \sum_a V^a_{loc}(|\mathbf{r}-\mathbf{R}_a|)|\psi_i\rangle + \sum_{a,l,m}\frac{|\phi^a_{l,m}\Delta V^a_l\rangle\langle\phi^a_{l,m}\Delta V^a_l|}{\langle\phi^a_{l,m}|\Delta V^a_l|\phi^a_{l,m}\rangle}|\psi_i\rangle \quad (2)$$

where $\mathbf{R}_a$ is the position vector of atom a, $\phi^a_{l,m}$ is the atomic pseudowave function of the angular momentum quantum number l,m, and ΔV^a_l is the difference between the l-dependent pseudopotential and the local pseudopotential V^a_{loc},

$$\Delta V^a_l = V^a_l - V^a_{loc}$$

The inner products of the nonlocal part of eq 2 are performed in the real space, while the long-range local parts are computed in the Fourier space. In this calculation we employed pseudopotentials NCPS 97 developed by the method of Troullier and Martins.[48,49] As a special treatment of the nonlocal pseudopotentials, we employ the double grid technique that enables us to realize the rapid behavior of the pseudopotentials near the atomic core regions.[15] The most important feature of the present double grid technique is that it requires only a modest increase of computational cost. This is because the wave functions on the dense grid points are simply computed by analytical interpolations of the wave functions on the coarse grid points as a benefit of the smooth nature of the pseudowave functions. In the previous work we employed the linear interpolations, while in the present work, four values on the original coarse grids are used for the Lagrange interpolation in 3 dimensions in order to obtain substantial accuracy. Within the Lagrange interpolation of four equally spaced points in 1-dimension, the wave function ψ_j on a dense grid point j is explicitly represented by the wave functions Ψ_J on the coarse grids as follows

$$\psi_j^J = \frac{(x_j^J - X_J)(x_j^J - X_{J+1})(x_j^J - X_{J+2})}{(X_{J-1} - X_J)(X_{J-1} - X_{J+1})(X_{J-1} - X_{J+2})}\Psi_{J-1} + \frac{(x_j^J - X_{J-1})(x_j^J - X_{J+1})(x_j^J - X_{J+2})}{(X_J - X_{J-1})(X_J - X_{J+1})(X_J - X_{J+2})}\Psi_J + \frac{(x_j^J - X_{J-1})(x_j^J - X_J)(x_j^J - X_{J+2})}{(X_{J+1} - X_{J-1})(X_{J+1} - X_J)(X_{J+1} - X_{J+2})}\Psi_{J+1} + \frac{(x_j^J - X_{J-1})(x_j^J - X_J)(x_j^J - X_{J+1})}{(X_{J+2} - X_{J-1})(X_{J+2} - X_J)(X_{J+2} - X_{J+1})}\Psi_{J+2} \quad (0 \le j \le n) \tag{3}$$

where n is the number of dense grid spacings between adjacent coarse grids, X_J are the coordinates of the Jth coarse grid, and x_j^J are those of the jth dense grid point related to X_J, respectively. The schematic representation of the relation between ψ_j^J and Ψ_J is presented in Figure 1.

Furthermore, in eq 3 it should be noted that one can get a simpler form when the relations $X_{J-1} - X_J = -h$, are adopted, where h is the coarse grid spacing. Once the wave functions on the dense grid points are computed, one can evaluate the inner product of the nonlocal part of eq 2 by a discrete sum over the dense grids,

$$\int \nu(x)\,\psi(x)\,\mathrm{d}x \approx \sum_J \sum_{j=0}^{n-1} \nu_j^J\,\psi_j^J h' \tag{4}$$

where h' denotes the grid spacing of dense grids, and ν_j^J is the value of $\phi_{l,m}^a\,\Delta V_l^a$ in eq 2 on the dense grid x_j^J. Substituting eq 3 into eq 4, we have

$$\sum_J \sum_{j=0}^{n-1} \nu_j^J\,\psi_j^J h' = \sum_J w_J \Psi_J h \tag{5}$$

where the weight factor w_J for the wave function Ψ_J becomes

$$w_J = \sum_{|j|=0}^{n} \frac{(h + |x_j^J - X_J|)(h - |x_j^J - X_J|)(2h - |x_j^J - X_J|)}{h \cdot h \cdot 2h}\nu_j^J + \sum_{|j|=n+1}^{2n} \frac{(h - |x_j^J - X_J|)(2h - |x_j^J - X_J|)(3h - |x_j^J - X_J|)}{h \cdot 2h \cdot 3h}\nu_j^J \tag{6}$$

in the case of the fourth-order Lagrange interpolations. What should be stressed here is that the weight factors expressed by eq 6 have to be computed *only once* before the SCF procedure and the computational cost during the SCF is almost the same as that for the original coarse grid calculation from the relation of eq 5. The dense grid spacing is taken as one-fifth of the coarse grid spacing h in this calculation. The h is set at 0.314 au, which is equivalent to a cutoff energy of 50 au for the planewave calculations. The electron exchange and correlation functional in eq 1 is evaluated from the local density approximation (LDA), and the equation used in the present calculation is that developed by Perdew and Zunger.[50] To examine the influence of the gradient corrections of the electron density on the potential energy, the BLYP functional is also employed.[51,52] In the course of the SCF procedure the wavefuctions are updated by the steepest descent (SD) algorithm. To expedite the SCF convergence, we utilize the preconditioning operator and perform the Rayleigh−Ritz corrections to updated wave functions. Consequently, a typical SCF procedure requires about 40 SD steps to get an energy convergence of 10^{-8} to 10^{-9} au. After every SCF step, Gram−Schmidt procedure is performed so that the orbitals $\{\psi_j\}$ obey the following orthogonalization constraints,

$$\langle \psi_i | \psi_j \rangle = \delta_{ij}$$

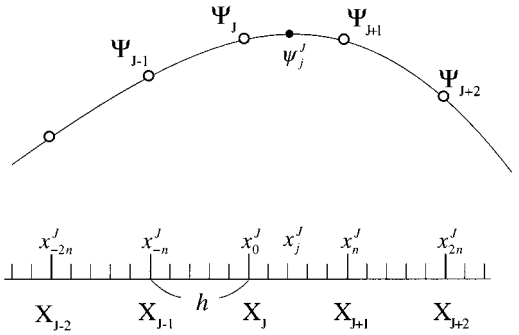

Figure 1. Schematic representation of the wave functions Ψ_J on the coarse grid points X_J and ψ_j on the dense grid points x_j^J. This figure shows a case when $n = 5$ and the coarse grid spacing is h.

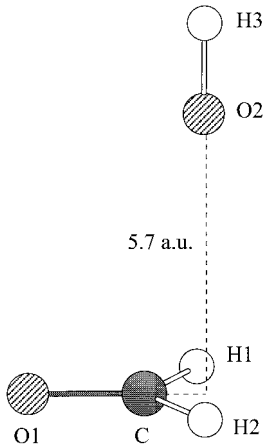

Figure 2. Schematic picture of the initial configuration of the formaldehyde and OH radical/OH anion system. The numbers are for later reference. The distance between the O2 atom and the molecular plane of formaldehyde is 5.7 au.

The initial configuration of the RS-AIMD simulation for the system HCHO and OH radical/OH ion is schematically drawn in Figure 2.

The OH molecule (OH radical or ion) is placed above the HCHO molecule in such a way that the OH bond is perpendicular to the HCHO plane and it crosses at the center of a line connecting the two H atoms of the HCHO molecule. This initial geometry is chosen somewhat arbitrarily; however, we take into account the electrostatic stability due to the fractional negative charge on the oxygen of the OH radical (or ion) and the positive charges on hydrogens of HCHO. The intermolecular distance, i.e., the distance between O2 atom and the HCHO plane, is determined so that the intermolecular interaction between the OH radical and formaldehyde is comparable to the thermal energy kT of the system, where temperature T is set at 300 K. In the sense that the simulation is done for the reactions in the supercritical water, the temperature should be set around its critical temperature of 647 K; however, we dare to do the simulations under the ambient temperature to see the effect of the molecular interactions on the dynamics clearly. The initial internal coordinates of formaldehyde are those experimentally obtained, while those of the OH radical (or ion) are determined by the DFT geometry optimization of Gaussian 98 with the B3LYP functional.[53,54] The basis set used for the optimization

TABLE 1: Molecular Internal Coordinates for Formaldehyde, OH Radical, and OH Ion[a]

parameter	expt[b]	ab initio
C−H1	2.109	
C−O1	2.283	
∠H1−C−H2	116.5	
O2−H3(radical)		1.851
O2−H3(ion)		1.858

[a] This work. Units are au and degrees for bond lengths and angles, respectively. [b] Reference 55.

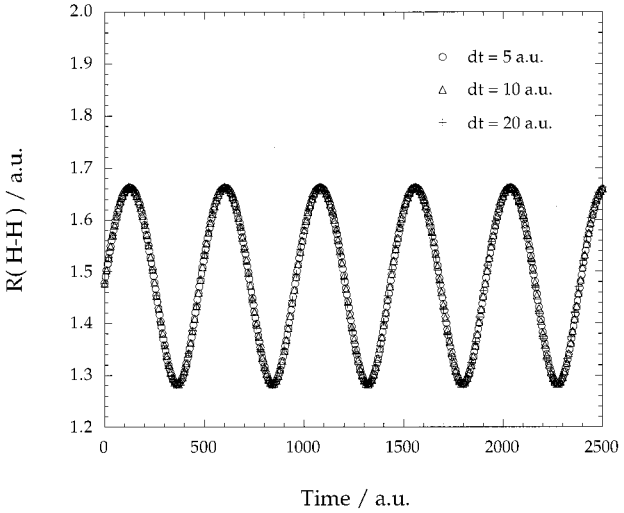

Figure 3. Variations of H−H distance as a function of time given by the RS-AIMD simulations. The open circles, triangles, and crosses correspond to the simulations that employ the MD time step of 5, 10, and 20 au, respectively. Kinetic energies equivalent to 600 K were given for the simulations.

is 6-31G augmented by polarization functions. The initial internal coordinates of the reactants are summarized in Table 1.

The SCF procedure by the SD scheme is repeatedly performed to obtain the electronic ground state of the system from which Hellmann−Feynman forces acted on nuclei are calculated. The MD simulations are performed by the velocity−Verlet algorithm with the time step of 20 au (0.484 fs). The temperature of the system is associated with the nuclear kinetic energy and the constant temperature simulation is achieved by rescaling the velocity after every 50 MD steps. The random values on the Gaussian distribution are assigned to the initial velocities of the nuclei and they are scaled so that T becomes 300 K. Calculations are done using a cubic periodic simulation cell of the size $L = 20.1$ au.

III. Results and Discussion

Preliminary Calculation. To test the efficiency of the present RS-AIMD code, we check the vibrational motion of the hydrogen molecule. At first two hydrogen atoms are placed at the distance optimized by the functional proposed by Perdew and Zunger and then they are given the translational velocities of the same size in the opposite direction to make the molecule vibrate. Translational kinetic energy is 600 K and no velocity rescaling is carried out throughout the simulations. The time profiles of the H−H distance provided by the RS-AIMD simulations are plotted in Figure 3 for the various time steps of velocity−Verlet algorithm ($\Delta t = 5$, 10, and 20 au).

The figure shows that the vibrational motion comes out soundly for each time step simulation. The amplitude of vibration is conserved during the simulation time up to 2500 au, indicating that the total energy of the system is completely conserved. This proves that the Hellmann−Feynman force calculations are correctly performed as well as the velocity−Verlet algorithm. Further, one can say that the molecular dynamics is not affected by the choice of the MD time step Δt at least in the range from 5 to 20 au because of the fact that the three trajectories at different time steps coincide strictly. This results ensures the accuracy of the present RS-AIMD simulations employing a time step of 20 au

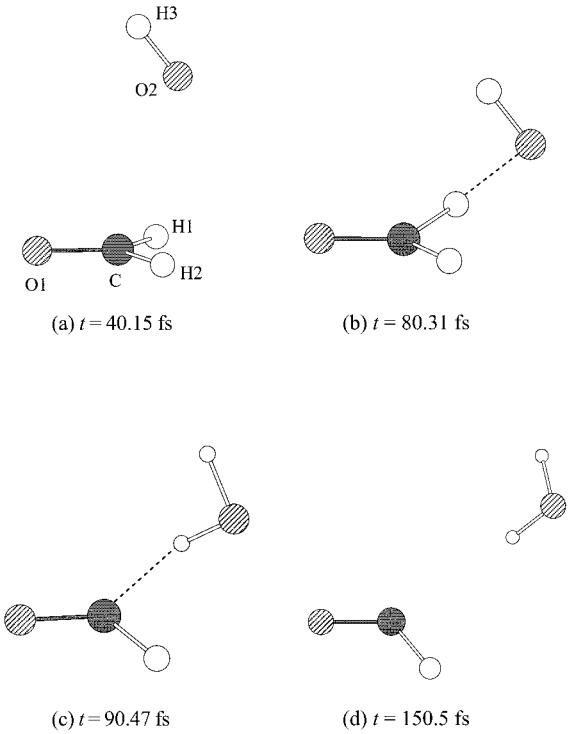

Figure 4. Snapshots of ab initio molecular dynamics simulation for formaldehyde and OH radical at (a) $t = 40.15$ fs, (b) $t = 80.31$ fs, (c) $t = 90.47$ fs, and (d) $t = 150.5$ fs, respectively. Broken lines are drawn between the weakly bonded atoms whose distance is smaller than 3.0 au.

HCHO and OH Radical. We first performed the simulation of the radical reaction in order to investigate the reaction dynamics and to see whether there exists a potential energy barrier for this reaction. When there exists a substantial height of potential energy barrier, the reaction will not occur in the ab initio molecular dynamics simulations unless the initial kinetic energy is sufficient enough to overcome the barrier. The snapshots along a reaction pathway obtained in this RS-AIMD simulation are depicted in Figure 4a−d.

Figure 4a shows a molecular configuration after 40 fs, in which we can recognize that the OH radical is substantially tilted because the negative charge on the C═O bond of HCHO attract the positively charged hydrogen of the OH radical. At about $t = 80$ fs, one of the hydrogens of HCHO is approaching the OH radical, as shown by the broken line, and the C−H1 bond of HCHO is stretching (Figure 4b). The hydrogen abstraction reaction from HCHO to OH radical takes place after about 90 fs (Figure 4c). Figure 4d shows that the strained H_2O molecule formed in the reaction is relaxed to its stable geometry. To clarify the quantitative behavior of the reaction dynamics, the potential energy of the system, the internal bond length, and the atom−atom distances are plotted as functions of time in Figure 5a,b.

Figure 5a shows the time profile of the potential energies along the reaction pathway, in which the corresponding mo-

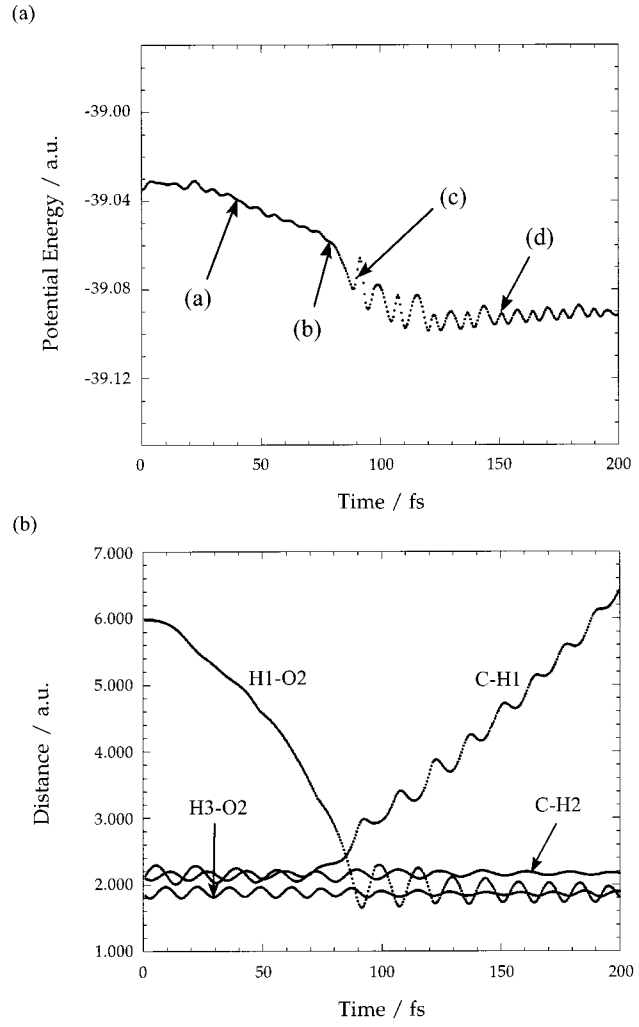

Figure 5. Time profiles of (a) the potential energy and (b) the atom−atom distances of interest for the radical process, recpectively. Each of the arrows (a), (b), (c), and (d) in (a) indicates the point that corresponds to molecular snapshot (a), (b), (c), and (d) in Figure 4, respectively.

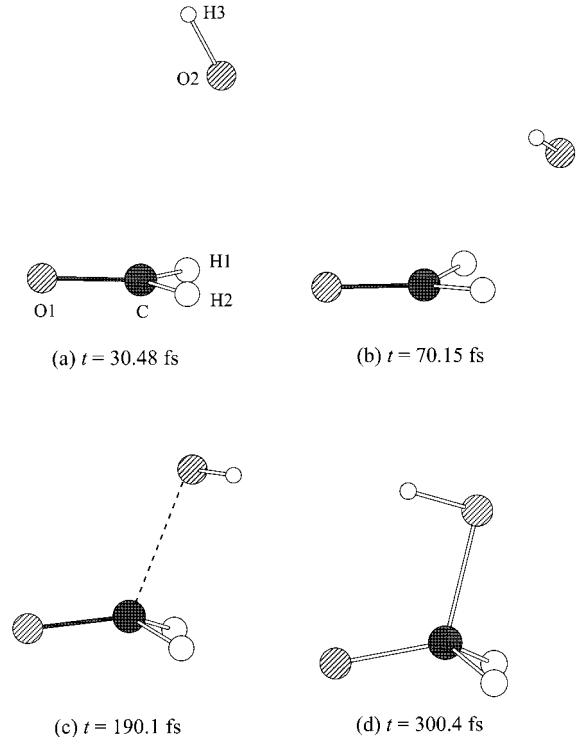

Figure 6. Snapshots of ab initio molecular dynamics simulation for formaldehyde and OH anion at (a) $t = 30.48$ fs, (b) $t = 70.15$ fs, (c) $t = 190.1$ fs, and (d) $t = 300.4$ fs, respectively. Broken lines are drawn between the weakly bonded atoms whose distance is smaller than 3.0 au.

lecular configurations in Figure 4a−d are indicated by the arrows. At first we have to note that there are no substantial potential energy barriers in this reaction within the level of LDA, though there exist small oscillations in the potential energy barriers that are comparable to kinetic energies. The potential energy begins to fall significantly around 70 fs accompanied by the C−H1 bond cleavage (Figure 5a,b). It is noticeable that the C−H2 bond vibration is almost unperturbed during the chemical bond exchange. The vibration of the newly formed H1−O2 bond is highly activated, which leads to the significant potential energy oscillations. Another OH bond of H_2O vibrates constantly during the reaction, and no intramolecular vibrational redistribution (IVR) can be observed in this time scale. The heat of the reaction was computed by subtracting the energy of the reactants from that of products by employing the nonperiodic simulation cells to eliminate the interactions from outer cells. The heat of reaction for the radical process based on the LDA calculation is 39.2 kcal/mol, while that determined by experiment is 33.2 kcal/mol.[36] The LDA calculation overestimates the reaction energy by 6 kcal/mol. To examine the effect of the gradient correction on the exchange and electron correlation, additional calculation was performed by employing the BLYP functional. The heat of reation computed by the BLYP functional is 33.3 kcal/mol, which is much closer to the experimental value than that of LDA calculation.

HCHO and OH Anion. In the same way as the radical process we have studied the dynamics of the nucleophilic addition of the OH anion to formaldehyde starting from the same molecular configuration and velocities. The snapshots of molecular dynamics are shown in Figure 6a−d.

Figure 6a is the molecular configuration after about 30 fs. The OH anion is tilted in the same way as in the case of the OH radical due to the electrostatic attractive force between the negative charge on the carbonyl group and the positive charge on the hydrogen of OH anion. After about 70 fs, the OH^- and the HCHO molecule make a complex with a long C−O2 distance (∼4.5 au). In Figure 7a,b one can see that the C−O2 distance and the potential energy of the system remain almost constant during the time from $t = 50$ to 150 fs, indicating that the complex persists during the time.

Existence of such a complex is also predicted in the literature,[45,46] in which it is noted that the complex is separated by a small barrier (∼1 kcal/mol) from a global minimum structure. After 150 fs, the OH^- again begins to approach the HCHO molecule. At about 190 fs, we found obvious deformation of HCHO from planar to tetrahedral configuration, accompnied by the hybridization change of carbon in HCHO from sp^2 to sp^3 (Figure 6c). The direction of the OH^- approach is consistent with the shape of Fukui function of HCHO for the nucleophilic attack.[56] Once the bond between the carbon and oxygen of the OH anion is formed, the OH bond moves so that the direction of the O2−H3 bond coincides with the C−O1 bond direction in order to gain the electrostatic stabilization energy. After about 300 fs, we obtain the relaxed tetrahedral complex formed by addition of OH anion to HCHO, where the O2−H3 bond is almost in the same plane with C−O1 bond (Figure 6d). The heat of reaction ΔE for the ionic process computed in the

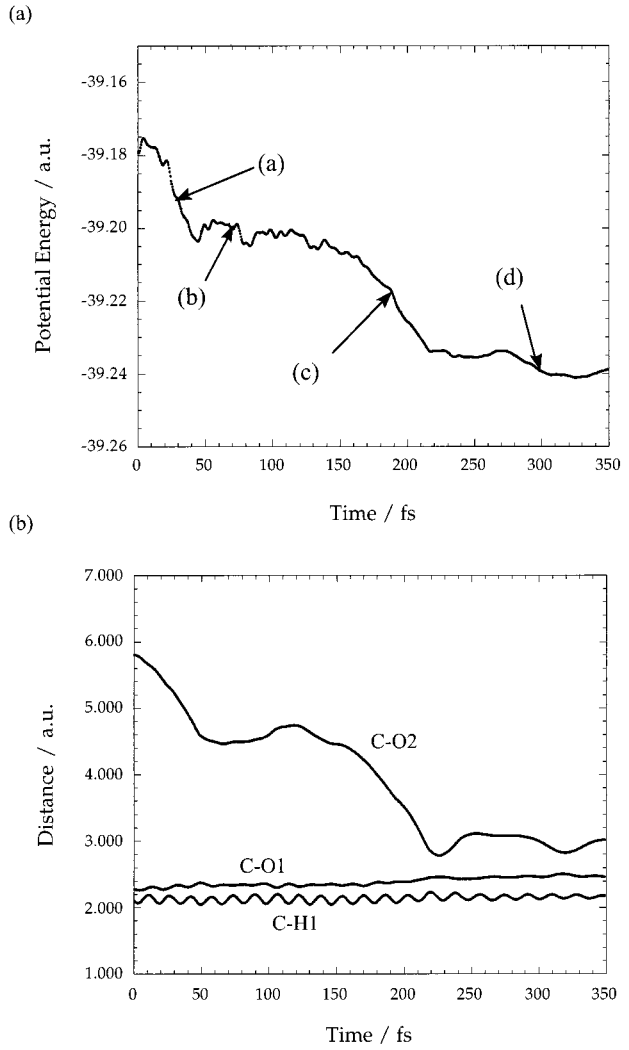

Figure 7. Time profiles of (a) the potential energy and (b) the atom−atom distances of interest for the ionic process, recpectively. Each of the arrows (a), (b), (c), and (d) in (a) indicates the point that corresponds to molecular snapshot (a), (b), (c), and (d) in Figure 6, respectively.

same way as the radical process is 50.9 kcal/mol within the LDA, while that obtained by the BLYP functional is 31.8 kcal/mol. It is surprising that the inclusion of the gradient corrections greatly diminishes ΔE for the ionic process. The discrepancy may be mainly attributed to the nature of the LDA, which generally overestimates the binding energy of chemical bonds. Also in ref 46, it is indicated that the heat of this reaction is very sensitive to the inclusion of the diffuse functions in the basis sets as well as the computational methods and it varies more than 30 kcal/mol dependent on the methods and basis sets. They noted that their best estimate of the energy release on forming tetrahedral complex is roughly 35 kcal/mol, which is almost comparable to the BLYP result in this work.

Comparison. Here we discuss the difference of the reactivity and the reaction dynamics between the OH radical and OH anion in the isolated conditions. As for the energy profile of the reaction of HCHO and OH anion, the most important feature to note is that the energy gradient is larger than that of the radical process. This implies that the ionic reaction process is driven by the long-range interaction forces, which is partially because of the electrostatic interaction due to the ion−dipole interaction between OH^- and HCHO molecule and partially because of the diffuse nature of the excess electron on the OH, which allows molecular orbitals to overlap even at a long distance. As compared with the ionic process, such effects are greatly diminished in the radical process since the molecular orbitals of the OH radical is not broadened and the OH radical is neutral. As has been shown in Figure 5a,b, the gradient of the potential energy with respect to the approach of the OH radical to formaldehyde is rather gentle. In this respect, the H-abstraction reaction by the OH radical will be less advantageous than the formation of the tetrahedral complex by the OH anion because the radical process will be initiated by the short-range interactions. On the basis of these results where no solvent molecule is involved, we can speculate how the polar solvent, such as ambient water, affects the reaction dynamics of the two processes. Surrounded by a polar solvent, the $HCHO-OH^-$ complex will be less stabilized than the OH anion since the negative charge may be more disperse in $HCHO-OH^-$ complex than OH anion. That is because spatially larger ionic species will be less stabilized by a polar solvent than smaller ones according to Born's equation. In ref 46 Jorgensen et al. performed Monte Carlo calculations for this system in the aqueous phase and predicted that $HCHO-OH^-$ will be destabilized as compared with reactants, though the solute's electronic polarization is not explicitly considered. In this respect, the ionic process will be deactivated in the ambient water solution because of its large dielectric constant ($\epsilon = 78.3$ at $T = 298$ K), while the radical process will not be so affected by the water solvent since the solvation energy will not be significant for both the reactant and product system. It is therefore reasonable to consider that the ionic process will play an important role in the supercritical region of water where the dielectric constant is smaller. On the contrary, in the ambient conditions the ionic process would be significantly suppressed and the radical process will become important.

Spin Polarization Effect in Radical Process. In general, radical species and radical processes inevitably undergo spin polarization effects to some extent, which leads to the spin contamination in the wave function when broken-symmetry approach is employed. Though the broken-symmetry problem can be avoided by the novel interpretation proposed by Perdew within the DFT formalism,[57] it would be better to examine the spin contamination effect for the radical process by molecular orbital (MO) theories. The multiconfiguration self-consistent field (MCSCF) approach[58,59] using spin-restricted open shell Hartree−Fock (ROHF) wave functions[60] will be the most suitable candidate that can properly calculate the energies for the bond formations and breakings. But in this method there are some ambiguities on the choice of the active space to which electrons are distributed unless full valence space calculation is feasible. The MCSCF calculations involving a large number of electrons distributed in the large active space is too expensive and only available for small molecules. The alternative approach is to calculate the correlation energy by perturbational theory, such as the Møller−Plesset (MP) perturbation method using the broken symmetry unrestricted Hartree−Fock (UHF) reference state, from which the spin contamination is eliminated by a spin-projection operator in the subsequent calculation.[61−63] It has been shown that this method can efficiently calculate the potential energy curves for the bond dissociations to some extent.[63]

To examine the dependence of the computational approach on the energetics, we perform several additional calculations using the Gaussian package along the reaction coordinate that has been obtained by the present AIMD simulation employing the BLYP functional. One is the spin-projected unrestricted fourth-order MP calculation with single, double, triple, and quadruple substitutions (PUMP4(SDTQ)), where all the valence

TABLE 2: Optimal Geometries for the [HCHO−OH]⁻ System[a]

	bond lengths (Å)				bond angles (deg)			
method	C−O1	C−H1	C−O2	O2−H3	O1−C−H1	O1−C−O2	H1−C−O2	C−O2−H3
				This Work				
PZ	1.307	1.146	1.514	0.986	116.6	112.9	101.9	95.05
BLYP	1.309	1.130	1.553	0.975	117.2	111.6	101.4	95.03
				LCAO				
BLYP[b]	1.293	1.174	1.569	0.985	118.0	112.9	101.1	94.09
BLYP[c]	1.315	1.140	1.589	0.979	116.4	112.5	100.9	97.53
MP2[b]	1.293	1.154	1.518	0.972	117.5	112.3	102.2	93.38
MP2[c]	1.322	1.128	1.539	0.972	115.7	112.0	102.1	96.47
HF[d]	1.365	1.090	1.527	0.968	114.9	110.6	103.1	103.3

[a] The numbers on atoms refer to those in Figure 6. [b] LCAO calculations (BLYP and MP2) are carried out by Gaussian 98 with the cc-pVDZ basis set. [c] LCAO calculations (BLYP and MP2) are carried out by Gaussian 98 with the AUG-cc-pVDZ basis set. [d] Reference 45.

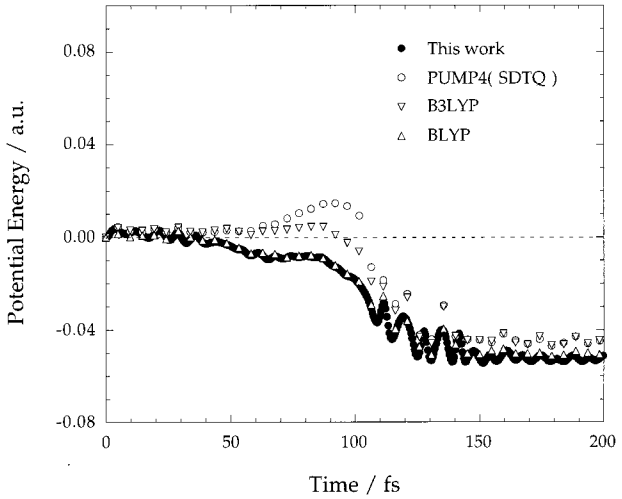

Figure 8. Potential energies computed by the PUMP4 (SDTQ) method, B3LYP, and BLYP functional along the reaction coordinate obtained by RS-AIMD simulation with the BLYP functional. Each of the energies for all the calculations is shifted so that the energy at the initial configuration ($t = 0$) becomes zero.

electrons are correlated and the others are DFT calculations with BLYP and B3LYP functionals. The BLYP functional is employed to check the accuracy of the present RS-AIMD method, and the B3LYP is applied to get higher accuracy within the DFT approach. The basis function is the correlation-consistent polarized valence orbital basis set of double-ζ quality augumented by diffuse functions (AUG-cc-pVDZ).[64] The results are summarized in Figure 8.

The most remarkable feature is that there appears a potential energy barrier in the PUMP4 (SDTQ) calculation. Also in ref 65 it has been shown that there exists a small energy barrier (1.2 kcal/mol) in this reaction by a transition state (TS) analysis of the PUMP4 (SDTQ)/6-311++G** calculation. Overestimation of the energy barrier of the present PUMP4 (SDTQ) calculation (∼10 kcal/mol) will mainly come from the fact that the molecular trajectory obtained by the AIMD simulation based on the BLYP functional missed the TS structure of ref 65. Further, it should be also noted that the discrepancy between B3LYP and PUMP4 approach is significant near the TS, though they strictly coincide with each other at the reactant and product states. These results indicate that the potential energies computed by DFTs are rather different from those computed by MO theory, PUMP4 (SDTQ), at the region where spin contamination is significant. Actually, the value of $\mathbf{S}^2$ becomes about 0.8 at $t = \sim 100$ fs in the UHF calculation. Also in ref 63 it is demonstrated that the energy of PUMP4-Full CI (configuration interaction) becomes large near the onset of spin contamination for several bond-dissociating systems. Therefore, it is possible that the PUMP4 calculation slightly overestimates the barrier height. The activation energy obtained by recent experimental observation for this reaction is -0.05 ± 0.30 kcal/mol, indicating that the reaction proceeds with almost no barrier.[36] Although it is a very subtle problem whether an energy barrier exists or not for this reaction, it will be valid to say that the barrier is very small even if it exists.

It is worthy of note that the energies of the present RS-AIMD method with BLYP functional coincide quite accurately with those of the Gaussian DFT calculation with the same functional, indicating that the RS-AIMD method has comparable accuracy with the Gaussian package with a highly sophisticated basis function, AUG-cc-pVDZ. The remarkable feature of the BLYP results is that the potential energy near the TS region is lower than those obtained by B3LYP and PUMP4 (SDTQ) calculations. It is possible that the stabilization energy near the TS is somewhat exaggerated, but the behavior of the potential energy of the BLYP functional is qualitatively satisfactory.

Geometry Optimizations. Further, to substantiate the efficiency of the calculation of the Hellmann−Feynman forces within the real space grid scheme, we carried out the geometry optimizations for the ionic complex [HCHO−OH]⁻. The optimized parameters are compared with those obtained by linear combination of atomic orbitals methods (LCAO). The geometry optimizations by the LCAO method are done by Gaussian 98 employing the DFT and the molecular orbital (MO) theory with comparable accuracy. The gradient-corrected exchange and correlation energy is estimated by the BLYP functional in the DFT calculations, and the MP2 theory is employed in the MO calculations to take into account the electron correlations, in which all valence electrons are correlated. Since it is reported that the addition of the diffuse functions in the basis set substantially affects the formation energy for this complex,[46] two sets of basis functions are used to see the effect of the diffuse basis functions on the geometry optimizations. One is the correlation-consistent polarized valence orbital basis set of double-ζ quality (cc-pVDZ) and another is that augumeted by diffuse functions (AUG-cc-pVDZ).[64]

The optimized bond lengths and the bond angles are summarized in Table 2, in which those from ref 45 are also referenced. The optimal geometry obtained by PZ functional is almost comparable with that obtained by the BLYP functional, indicating that the gradient correction does not give significant effects on the determination of the optimal geometry for this system. As for the LCAO calculations by Gaussian 98, it can be said that the DFT/BLYP calculation gives similar results as the MO/MP2 theory. The addition of diffuse functions gives slight but similar effects on the optimal parameters for the DFT and MO calculations. For example, C−O1 and C−O2 distances

and the C−O2−H3 angle are enlarged by the addition of the diffuse functions for both methods. It is also worthy of note that HF-SCF calculation with the 3-21G basis set[45] shows rather good results as compared with those of the state-of-the-art.

The comparison between the real space grid approach with the BLYP functional and the LCAO methods with diffuse basis functions reveals that the diffecences in the optimized values between them are less than 2%. In this respect, it appears that the real space grid method reinforced by the double grid technique is adequate for the computation of the Hellmann−Feynman force as well as that of the potential energy of the system.

IV. Conclusions

In the present work, we developed a code for real space ab initio molecular dynamics simulations reinforced by the double grid technique. We applied the method to the simulation of the reaction of formaldehyde and the OH radical/OH^- ion to investigate the reactivities in the supercritical water solvent. Our simulations show that both reactions proceed without potential energy barriers within the LDA and GGA level. It is confirmed that the H-abstraction reaction by the OH radical takes place in the radical process and the tetrahedral complex is formed in the ionic process. It is also found that the ionic process is driven by the long-range interaction forces in contrast with the radical process.

The computed heat of reaction for the radical process agrees with the experimental value within 1 kcal/mol and the optimized geometry of the $[HCHO-OH]^-$ complex is in good agreement with that obtained by LCAO methods, indicating that the present approach is adequate for the ab initio molecular dynamics simulations.

Acknowledgment. This work has been supported by CREST (Core Research for Evolutional Science and Technology) of the Japan Science and Technology Corp. (JST). We thank Prof. K. Hirose and co-workers for the fruitful discussions on the real space double grid method.

Supporting Information Available: Table of energies of related species. This information is available free of charge via the Internet at http://pubs.acs.org.

References and Notes

(1) Hohenberg, P.; Kohn, W. *Phys. Rev. B* **1964**, *136*, 864.
(2) Kohn, W.; Sham, L. J. *Phys. Rev. A* **1965**, *140*, 1133.
(3) Ihm, J.; Zunger, A.; Cohen, M. L. *J. Phys. C* **1979**, *12*, 4409.
(4) Pickett, W. E. *Comput. Phys. Rep*. **1989**, *9*, 115.
(5) Chelikowsky, J. R.; Troullier, N.; Saad, Y. *Phys. Rev. Lett*. **1994**, *72*, 1240.
(6) Chelikowsky, J. R.; Troullier, N.; Wu, K.; Saad, Y. *Phys. Rev. B* **1994**, *50*, 11355.
(7) Jing, X.; Troullier, N.; Dean, D.; Binggeli, N.; Chelikowsky, J. R.; Wu, K.; Saad, Y. *Phys. Rev. B* **1994**, *50*, 12234.
(8) Hoshi, T.; Arai, M.; Fujiwara, T. *Phys. Rev. B* **1995**, *52*, 5459.
(9) Barnett, R. N.; Landman, U. *Phys. Rev. B* **1993**, *48*, 2081.
(10) Bernholc, J.; Briggs, E. L.; Sullivan, D. J.; Brabec, C. J.; Buongiorno Nardelli, M.; Rapcewicz, K.; Roland, C.; Wensell, M. *Int. J. Quantum Chem.* **1997**, *65*, 531.
(11) Briggs, E. L.; Sullivan, D. J.; Bernholc, J. *Phys. Rev. B* **1996**, *54*, 14362.
(12) Nardelli, M. B.; Yakobson, B. I.; Bernholc, J. *Phys. Rev. B* **1998**, *57*, R4277.
(13) Ogut, S.; Chelikowsky, J. R. *Phys. Rev. Lett*. **1999**, *83*, 3852.
(14) Ramamoorthy, M.; Briggs, E. L.; Bernholc, J. *Phys. Rev. Lett*. **1998**, *81*, 1642.
(15) Ono, T.; Hirose, K. *Phys. Rev. Lett*. **1999**, *82*, 5016.
(16) Takahashi, H.; Hori, T.; Wakabayashi, T.; Nitta, T. *Chem. Lett*. **2000**, *3*, 222.
(17) Cheng, H. P. *J. Phys. Chem. A* **1998**, *102*, 6201.
(18) Sprik, M.; Hutter, J.; Parrinello, M. *J. Chem. Phys*. **1996**, *105*, 1142.
(19) Lee, C.; Vanderbilt, D.; Laasonen, K.; Car, R.; Parrinello, M. *Phys. Rev. Lett*. **1992**, *69*, 462.
(20) Fois, E. S.; Sprik, M.; Parrinello, M. *Chem. Phys. Lett*. **1994**, *223*, 411.
(21) Laasonen, K.; Klein, M. L. *Mol. Phys*. **1996**, *88*, 135.
(22) Laasonen, K. E.; Klein, M. L. *J. Phys. Chem. A* **1997**, *101*, 98.
(23) Laasonen, K.; Sprik, M.; Parrinello, M.; Car, R. *J. Chem. Phys*. **1993**, *99*, 9080.
(24) Yamataka, H.; Aida, M. *Chem. Phys. Lett*. **1998**, *289*, 105.
(25) Yamataka, H.; Aida, M.; Dupuis, M. *Chem. Phys. Lett*. **1999**, *300*, 583.
(26) Wei, D.; Salahub, D. R. *J. Chem. Phys*. **1997**, *106*, 6086.
(27) Termath, V.; Sauer, J. *Mol. Phys.* **1997**, *91*, 963.
(28) Ortega, J.; Lewis, J. P.; Sankey, O. F. *J. Chem. Phys.* **1997**, *106*, 3696.
(29) Car, R.; Parrinello, M. *Phys. Rev. Lett.* **1985**, *55*, 2471.
(30) Ben-Nun, M.; Martinez, T. J. *Chem. Phys. Lett*. **1998**, *298*, 57.
(31) Martinez, T. J. *Chem. Phys. Lett.* **1997**, *272*, 139.
(32) Gibson, D. A.; Ionova, I. V.; Carter, E. A. *Chem. Phys. Lett*. **1995**, *240*, 261.
(33) Hartke, B.; Carter, E. A. *Chem. Phys. Lett*. **1992**, *189*, 358.
(34) Savage, P. E. *Chem. Rev.* **1999**, *99*, 603.
(35) Tsujino, Y.; Wakai, C.; Matubayashi, N.; Nakahara, M. *Chem. Lett*. **1999**, *4*.
(36) Butkovskaya, N. I.; Setser, D. W. *J. Phys. Chem. A* **1998**, *102*, 9715.
(37) Atkinson, R.; Baulch, D. L.; Cox, R. A., Jr.; Hampson, R. F.; Kerr, J. A.; Troe, J. *J. Phys. Chem. Ref. Data* **1992**, *21*, 1125.
(38) Guo, Y.; Smith, S. C.; Moore, C. B.; Melius, C. F. *J. Phys. Chem*. **1995**, *99*, 7473.
(39) Rim, K. T.; Hershberger, J. F. *J. Phys. Chem. A* **1998**, *102*, 5898.
(40) Timonen, R. S.; Ratajczak, E.; Gutman, D. *J. Phys. Chem.* **1988**, *92*, 651.
(41) Veyret, B.; Lesclaux, R. *J. Phys. Chem.* **1981**, *85*, 1918.
(42) Timonen, R. S.; Ratajczak, E.; Gutman, D. *J. Phys. Chem.* **1987**, *91*, 692.
(43) Wu, Y. D.; Houk, K. N. *J. Am. Chem. Soc*. **1987**, *109*, 906.
(44) Wu, Y. D.; Houk, K. N. *J. Am. Chem. Soc*. **1987**, *109*, 908.
(45) Cardy, H.; Loudet, M.; Poulicard, J.; Ollivier, J.; Poquet, E. *Chem. Phys.* **1989**, *131*, 227.
(46) Madura, J. D.; Jorgensen, W. L. *J. Am. Chem. Soc*. **1986**, *108*, 2517.
(47) Kleinman, L.; Bylander, D. M. *Phys. Rev. Lett*. **1982**, *48*, 1425.
(48) Kobayashi, K. In proceedings of the international workshop on Computer Modeling and Simulation for Material Design, 96 (1996).
(49) Troullier, N.; Martins, J. L. *Phys. Rev. B* **1991**, *43*, 1993.
(50) Perdew, J. P.; Zunger, A. *Phys. Rev. B* **1981**, *23*, 5048.
(51) Becke, A. D. *Phys. Rev. A* **1988**, *38*, 3098.
(52) Lee, C.; Yang, W.; Parr, R. G. *Phys. Rev. B* **1988**, *37*, 785.
(53) Frisch, M. J.; Trucks, G. W.; Schlegel, H. B.; Scuseria, G. E.; Robb, M. A.; Cheeseman, J. R.; Zakrzewski, V. G.; Montgomery, J. A., Jr.; Stratmann, R. E.; Burant, J. C.; Dapprich, S.; Millam, J. M.; Daniels, A. D.; Kudin, K. N.; Strain, M. C.; Farkas, O.; Tomasi, J.; Barone, V.; Cossi, M.; Cammi, R.; Mennucci, B.; Pomelli, C.; Adamo, C.; Clifford, S.; Ochterski, J.; Petersson, G. A.; Ayala, P. Y.; Cui, Q.; Morokuma, K.; Malick, D. K.; Rabuck, A. D.; Raghavachari, K.; Foresman, J. B.; Cioslowski, J.; Ortiz, J. V.; Stefanov, B. B.; Liu, G.; Liashenko, A.; Piskorz, P.; Komaromi, I.; Gomperts, R.; Martin, R. L.; Fox, D. J.; Keith, T.; Al-Laham, M. A.; Peng, C. Y.; Nanayakkara, A.; Gonzalez, C.; Challacombe, M.; Gill, P. M. W.; Johnson, B. G.; Chen, W.; Wong, M. W.; Andres, J. L.; Head-Gordon, M.; Replogle, E. S.; Pople, J. A. *Gaussian 98*, revision A.6; Gaussian, Inc.: Pittsburgh, PA, 1998.
(54) Becke, A. D. *J. Chem. Phys.* **1993**, *98*, 5648.
(55) Starck, B.; Vogt, J. *Microwave Catalogue and Supplements*; Van Nostrand Reinhold Co.: New York, 1979.
(56) Gilardoni, F.; Weber, J.; Chermette, H.; Ward, T. R. *J. Phys. Chem. A* **1998**, *102*, 3607.
(57) Perdew, J. P.; Savin, A.; Burke, K. *Phys. Rev. B* **1995**, *51*, 4531.
(58) Hegarty, D.; Robb, M. A. *Mol. Phys*. **1979**, *38*, 1795.
(59) Eade, R. H. A.; Robb, M. A. *Chem. Phys. Lett*. **1981**, *83*, 362.
(60) Roothaan, C. C. *Rev. Mod. Phys*. **1951**, *23*, 69.
(61) Knowles, P. J.; Handy, N. C. *J. Phys. Chem.* **1988**, *92*, 3097.
(62) Schlegel, H. B. *J. Phys. Chem.* **1988**, *92*, 3075.
(63) Chen, W.; Schlegel, H. B. *J. Chem. Phys.* **1994**, *101*, 5957.
(64) Dunning, T. H., Jr. *J. Chem. Phys.* **1989**, *90*, 1007.
(65) Francisco, J. S. *J. Chem. Phys.* **1992**, *96*, 7597.